HHS Public Access

Author manuscript

Brain Imaging Behav. Author manuscript; available in PMC 2017 June 01.

Published in final edited form as:

Brain Imaging Behav. 2016 June ; 10(2): 342–356. doi:10.1007/s11682-015-9408-2.

Sparse Temporally Dynamic Resting-State Functional Connectivity Networks for Early MCI Identification

Chong-Yaw Wee,
Image Display, Enhancement, and Analysis (IDEA) Laboratory, Biomedical Research Imaging Center (BRIC) and Department of Radiology, University of North Carolina at Chapel Hill, NC 27599, USA

Sen Yang,
Department of Computer Science and Engineering, Arizona State University, Tempe, AZ, USA

Pew-Thian Yap,
Image Display, Enhancement, and Analysis (IDEA) Laboratory, Biomedical Research Imaging Center (BRIC) and Department of Radiology, University of North Carolina at Chapel Hill, NC 27599, USA

Dinggang Shen[*], and
Image Display, Enhancement, and Analysis (IDEA) Laboratory, Biomedical Research Imaging Center (BRIC) and Department of Radiology, University of North Carolina at Chapel Hill, NC 27599, USA

Department of Brain and Cognitive Engineering, Korea University, Seoul, Republic of Korea

for the Alzheimer's Disease Neuroimaging Initiative[‡]

Abstract

In conventional resting-state functional MRI (R-fMRI) analysis, functional connectivity is assumed to be temporally stationary, overlooking neural activities or interactions that may happen within the scan duration. Dynamic changes of neural interactions can be reflected by variations of topology and correlation strength in temporally correlated functional connectivity networks. These connectivity networks may potentially capture subtle yet short neural connectivity disruptions induced by disease pathologies. Accordingly, we are motivated to utilize disrupted temporal network properties for improving control-patient classification performance. Specifically, a sliding window approach is firstly employed to generate a sequence of overlapping R-fMRI sub-series. Based on these sub-series, sliding window correlations, which characterize the neural interactions between brain regions, are then computed to construct a series of temporal networks. Individual

[*]Corresponding author: Dinggang Shen, dgshen@med.unc.edu, Tel.: +1 919-843-3535, Fax: +1 919-843-2641.

[‡]ADNI

Data used in preparation of this article were obtained from the Alzheimer's Disease Neuroimaging Initiative (ADNI) database (adni.loni.ucla.edu). As such, the investigators within the ADNI contributed to the design and implementation of ADNI and/or provided data but did not participate in analysis or writing of this report. A complete listing of ADNI investigators can be found at: http://adni.loni.ucla.edu/wp-content/uploads/how_to_apply/ADNI_Acknowledgement_List.pdf.

Financial Disclosures

There are no conflicts of interest including any financial, personal, or other relation-ships with people or organizations for any of the coauthors related to the work described in the article.

estimation of these temporal networks using conventional network construction approaches fails to take into consideration intrinsic temporal smoothness among successive overlapping R-fMRI subseries. To preserve temporal smoothness of R-fMRI sub-series, we suggest to jointly estimate the temporal networks by maximizing a penalized log likelihood using a fused sparse learning algorithm. This sparse learning algorithm encourages temporally correlated networks to have similar network topology and correlation strengths. We design a disease identification framework based on the estimated temporal networks, and group level network property differences and classification results demonstrate the importance of including temporally dynamic R-fMRI scan information to improve diagnosis accuracy of mild cognitive impairment patients.

Keywords

Mild Cognitive Impairment (MCI); Resting-state functional MRI (R-fMRI); sliding window correlation; temporal dynamics; temporal smoothness; sparse temporal networks

1 Introduction

There is ample literature that suggests the pathological manifestation of Alzheimer's disease (AD) begins many years or decades before any clinical symptom can be observed (Johnson et al, 2006; Thompson and Apostolova, 2007; Whitwell et al, 2007). When AD symptoms are observed, significant neurodegeneration has already occurred in the brain, either anatomically or functionally (Li et al, 2012; Wee et al, 2013; Zhang et al, 2012). Furthermore, if memory loss is the predominant symptom (Dubois and Albert, 2004; Economou et al, 2007; Han et al, 2012b; Tabert et al, 2006), patients with Mild Cognitive Impairment (MCI), an intermediate stage between the expected cognitive decline of normal aging and AD, have an increased risk of developing AD. This risk can be reduced if appropriate interventions and treatments are provided during the early stages of MCI. However, for MCI patients changes in the brain are very subtle (Johnson et al, 2006; Li et al, 2011; McEvoy et al, 2009; Smith et al, 2007), therefore the early detection of MCI in neuroimaging data (e.g., MRI and fMRI) can be very challenging.

Neuroimaging data has been widely used in AD and MCI analysis to explore brain structure atrophies and brain function disruptions to enhance our knowledge of the biological underpinnings of AD/MCI. Recently, resting-state functional MRI (R-fMRI) (Smith et al, 2011; Sporns, 2011; Stam et al, 2007; Supekar et al, 2008; Wang et al, 2010), which characterizes hemodynamic response related to neural activity, has been widely used because of its ability to detect patients with MCI or AD before the clinical symptoms (Sheline and Raichle, 2013). This early detection is achieved by identifying disrupted functional connectivity, which is related to neural activity, using a graph theoretic technique. Through this technique, disruptions in functional connectivity are primarily reflected in the disruptions of network topology and connection strengths, which propels the consideration of using R-fMRI as a potential biomarker to effectively detect early MCI (eMCI).

In conventional network-based analysis, it is assumed that correlations between different brain regions in a typical R-fMRI scanning session of approximately 5 ~ 10 minutes are not changing over time (i.e., *temporally stationary*) with a repetition time (TR) in the range of 2

~ 3 seconds. Because of this assumption, brain region correlations are computed over the entire duration of R-fMRI scan to characterize network connection strengths (Achard et al, 2006; Dosenbach et al, 2007; Fransson and Marrelec, 2008; Greicius et al, 2004; Rombouts et al, 2005; Suk et al, 2013, 2014; Wee et al, 2012a,b, 2014). However, recent studies suggest that wealth of information is contained within the temporal features of spontaneous BOLD functional connectivity (Allen et al, 2014; Chang and Glover, 2010; Chang et al, 2013; Handwerker et al, 2012; Hutchison et al, 2013a; Jia et al, 2013; Smith et al, 2012; Tomasi et al, 2013) and functional connectivity metrics are able to index changes in temporal patterns of neural activity either in rest or task conditions (Hutchison et al, 2013a; Tomasi et al, 2013). Given the increasing evidence of dynamic functional connectivity during rest and its important for characterizing brain's intrinsic functional organization, multiple network estimation technique that can characterize fluctuations of whole-brain functional connectivity becomes necessary to better reveal connectivity patterns with *coherent dynamics*. In this paper, we suggest to use our recently proposed sparse leaning-based method to jointly estimate multiple temporally correlated networks, which simultaneously preserves the sparsity and coherent dynamics (temporal smoothness) among networks.

Recently, disease-related alterations in the dynamic properties of functional connectivity have been reported (Jones et al, 2012; Saköglu et al, 2010), further suggesting a neural origin and raising the intriguing possibility that temporal features of functional connectivity could serve as a disease biomarker. Inspiring by the advantages of the previous mentioned findings, we hypothesize that the dynamic patterns of whole-brain functional connectivity of R-fMRI and thus their network properties derived based on graph theory may be disrupted by disease pathologies. Motivated by this hypothesis, we design a novel framework that utilizes a series of temporal functional connectivity networks derived from an R-fMRI scan to possibly improve disease identification performance between eMCI patients and healthy controls. The novelty is three-fold: 1) a temporal series of sparse functional connectivity networks (*sparse temporal networks* for short) are constructed to estimate the time varying dynamic properties of functional connectivity over the duration of R-fMRI scan, 2) sparse temporal networks are estimated simultaneously to preserve temporal smoothness, i.e. temporally adjoint sparse networks have similar topology and connection strengths, 3) a network measure-based framework is proposed to improve patient-control identification performance.

The rest of the paper is organized as follows: Section 2 provides detailed descriptions on the proposed temporal network-based disease identification framework and the dataset used in this study. Performance of the proposed framework is evaluated extensively in Section 3. Findings, methodological issues, and limitations of the proposed framework are discussed in Section 4. Section 5 concludes this study.

2 Material and Methods

2.1 Participants and Data Acquisition

Data used in this study were obtained from the ADNI dataset[1]. The primary goal of ADNI was to test whether serial MRI, positron emission tomography (PET), other biological

markers, and clinical and neuropsychological assessment can be combined to measure the progression of MCI and early AD. Determination of sensitive and specific markers of very early AD progression is intended to aid researchers and clinicians to develop new treatments and monitor their effectiveness, as well as lessen the time and cost of clinical trials. A more detailed description of the ADNI dataset is provided in Appendix A.

Twenty nine eMCI subjects (13F/16M) and 30 normal controls (NCs) (17F/13M) were obtained from ADNI 2 dataset. Subjects from both groups are age-matched ($p = 0.6174$), with mean age in terms of year for eMCI and NC groups as 73.6 ± 4.8 and 74.3 ± 5.7, respectively. All subjects were scanned at different centers using 3.0 T Philips Achieva scanners with the following parameters: TR/TE = 3000/30 mm, flip angle = 80°, imaging matrix = 64 × 64, 48 slices, 140 volumes, and voxel thickness = 3.3 mm. Standard R-fMRI preprocessing procedure was performed using the SPM8 software package[2]. The first 10 acquired R-fMRI volumes of each subject were initially discarded before any further processing to ensure magnetization equilibrium. The remaining 130 volumes were then corrected for the staggered order of slice acquisition that was used during echo-planar scanning. The correction ensures the data on each slice correspond to the same point in time. The interpolated time point was chosen as the TR/2 time to minimize relative errors across each TR in the study. After acquisition time delay correction, the slice timing corrected R-fMRI time-series of each subject were realigned using a least squares approach and a rigid body spatial transformation. The first volume of each subject was used as the reference to which all subsequent volumes were realigned. This step removed the head-motion artifacts in the R-fMRI time-series. There were no significant group differences in head-motion for all participants used in the study. After realignment, the volumes were resliced such that they match the first volume voxel-by-voxel. R-fMRI images were then normalized to the MNI space with resolution of $3 \times 3 \times 3$ mm^3.

To further reduce the effects of nuisance signals before inferring functional connectivity, regression of ventricle and WM signals as well as six head-motion profiles was performed (Van Dijk et al, 2010). Given the controversy of removing the global signal in the post-processing of R-fMRI data (Fox et al, 2009; Murphy et al, 2009), we did not regress the global signal out (Achard et al, 2006; Lynall et al, 2010; Supekar et al, 2008). The regressed R-fMRI images were parcellated into 116 regions-of-interest (ROIs) according to the Automated Anatomical Labeling (AAL) template (Tzourio-Mazoyer et al, 2002). Prior to functional connectivity estimation, mean R-fMRI time series of each ROI was band-pass filtered ($0.01 \leq f \leq 0.08$Hz).

2.2 Proposed Framework

The proposed sparse temporal network-based disease identification framework is graphically shown in Figure 1. Specifically, for each ROI entire mean time series of an R-fMRI scan is decomposed into multiple overlapping sub-series using a sliding window (Allen et al, 2014; Chang and Glover, 2010; Handwerker et al, 2012; Smith et al, 2012) where its length shorter than the duration of the R-fMRI scan. For each R-fMRI sub-series, correlation coefficients

[1] http://www.adni-info.org
[2] http://www.fil.ion.ucl.ac.uk/spm/software/spm8/

between different brain regions are computed to generate one functional connectivity network. Sparse temporal networks are estimated simultaneously from these sub-series using fused multiple group LASSO (FMGL) to preserve the temporal smoothness between adjoining networks. Network measure, i.e., local clustering coefficients, are calculated from each sparse temporal network. Local clustering coefficients of all temporal networks are then concatenated into a long feature vector to train a Support Vector Machine (SVM) classifier.

2.3 Functional Connectivity Estimation

Generation of multiple R-fMRI sub-series using the sliding window approach is graphically illustrated in Figure 2. In particular, given an R-fMRI time series with M temporal image volumes, $K = \lfloor (M - N)/s \rfloor + 1$ is the number of sub-series that can be generated, where N denotes the length of sliding window and s denotes the translation step size. The k-th sub-series is represented in the form of a matrix $\mathbf{X}^{(k)}=\{\mathbf{x}_1^{(k)}, \mathbf{x}_2^{(k)}, \ldots, \mathbf{x}_P^{(k)}\} \in \mathbb{R}^{N\times P}$, k=1,…, K, where P = 116 is the total number of regions-of-interest (ROIs), and $\mathbf{x}^{(k)} = [x^{(k)}(1), x^{(k)}(2), \ldots, x^{(k)}(N)]^T$ is the k-th sub-series of N image volumes for a particular ROI. A symmetric connectivity matrix $\mathbf{C}^{(k)}= \left[C_{i,j}^{(k)}\right] \in \mathbb{R}^{P\times P}$ can be constructed using $\mathbf{X}^{(k)}$, where each element in the connectivity matrix defines the correlation strength between two different ROIs. Specifically, the correlation strength is defined as

$$C_{ij}^{(k)}=\mathrm{corr}\left(\mathbf{x}_i^{(k)}, \mathbf{x}_j^{(k)}\right), \quad (1)$$

where i and j are two different brain regions, and $corr(\cdot)$ computes the correlation between region i and region j. For instance, if i = 1 and j = 2 Eq. (1) would compute the correlation strength between regions 1 and 2 for sub-series k. It is noteworthy that the conventional stationary-based functional connectivity matrix can be estimated by replacing $corr(\cdot)$ in Eq. (1) with Pearson or partial correlations and K = 1.

2.4 Graphical Model

Assuming that the image volumes within each R-fMRI sub-series are identically distributed with P-variate Gaussian distribution with zero mean and positive definite covariance matrix $\Sigma^{(k)}$. Due to sparse nature of brain network, there should be many conditionally independent connection pairs. These null connections are denoted as zero elements in the precision matrix, i.e., network matrix $\Theta^{(k)} = (\Sigma^{(k)})^{-1}$. If the covariance matrix of each $\mathbf{X}^{(k)}$ is $\mathbf{S}^{(k)} = (1/N)(\mathbf{X}^{(k)})^T\mathbf{X}^{(k)}$, then the negative log likelihood of $\Theta^{(k)}$ is given as

$$\mathcal{L}(\Theta)=\sum_{k=1}^{K}\left(-\log\det(\Theta^{(k)})+tr(\mathbf{S}^{(k)}\Theta^{(k)})\right), \quad (2)$$

where $\Theta = \{\Theta^{(1)},\ldots, \Theta^{(K)}\}$. Minimizing Eq. (2) leads to the maximum likelihood estimate (MLE) of $\hat{\Theta^{(k)}} = (\mathbf{S}^{(k)})^{-1}$, which is unlikely to be sparse. Eq. (2) can then be solved by minimizing the penalized negative log likelihood as

$$\min_{\Theta^{(k)}\succ 0, k=1,\ldots,K} \mathcal{L}(\Theta)+Q(\Theta), \quad (3)$$

with $Q(\Theta)$ to be defined in following subsections.

2.5 Sparse Inverse Covariance Estimation

To model brain connectivity matrix, which has been proven to be sparse (Kötter and Stephen, 2003; Sporns et al, 2004), a "sparsity" constraint can be imposed on the MLE of an precision matrix using sparse inverse covariance matrix (SICE) (Huang et al, 2010), which also known as Gaussian graphical models or graphical LASSO. In SICE, the second term in Eq. (3), $Q(\Theta)$, is defined as (Huang et al, 2010)

$$Q(\Theta)=\lambda\sum_{k=1}^{K}\sum_{i\neq j}|\theta_{i,j}^{(k)}|, \quad (4)$$

where λ is a nonnegative regularization parameter. ℓ_1-norm in Eq. (4) is imposed to the elements of K networks, producing matrices with different non-zero locations.

2.6 Group Graphical Lasso

Estimating multiple networks individually fails to capture the temporal smoothness among adjoining networks. This problem can be partially solved by using joint estimation methods such as Group Graphical Lasso (GGL) (Danaher et al, 2012), which estimates multiple networks simultaneously. In GGL, the last term of Eq. (3) is defined as (Danaher et al, 2012)

$$Q(\Theta)=\lambda_1\sum_{k=1}^{K}\sum_{i\neq j}\left|\theta_{i,j}^{(k)}\right|+\lambda_2\sum_{i\neq j}\sqrt{\sum_{k=1}^{K}\left(\theta_{i,j}^{(k)}\right)^2}, \quad (5)$$

where λ_1 and λ_2 are non-negative regularization parameters. The second term of Eq. (5), a $\ell_{2,1}$-norm constraint, is applied to the (i, j) elements across all networks. This penalization forces an identical pattern of sparsity across all networks, i.e., same non-zero locations in K estimated networks, overlooking temporal smoothness between adjoining temporal networks.

2.7 Fused Multiple Graphical LASSO

Drawbacks of SICE and GGL methods can be solved by employing our recently proposed sparse learning algorithm, i.e., Fused Multiple Graphical LASSO (FMGL) algorithm (Yang et al, 2012). FMGL simultaneously estimates a series of temporal networks by replacing the last term in Eq. (3) with following term (Yang et al, 2012)

$$Q(\Theta)=\lambda_1\sum_{k=1}^{K}\sum_{i\neq j}\left|\theta_{i,j}^{(k)}\right|+\lambda_2\sum_{k=1}^{K-1}\sum_{i\neq j}\left|\theta_{i,j}^{(k)}-\theta_{i,j}^{(k+1)}\right|.$$

In particular, an ℓ_1-norm penalization is imposed to induce network sparsity (Achard and Bullmore, 2007; Chen et al, 2012; Friedman et al, 2008) and a fused regularization is imposed to preserve the temporal smoothness by encouraging $\Theta^{(k)}$ to have similar topology and correlations strengths to its adjoining networks (Tibshirani et al, 2005). FMGL was implemented using an in-house software.

2.8 Network Analysis

One of the important properties of human brain network is small-worldness. Since multiple sparse networks are generated to extract the temporally dynamic characteristics of brain functional connectivity, it is of great important to ensure that the generated networks are small-world networks instead of random or lattice-like networks. Accordingly, we use two network measures, i.e., small-world coefficient (Humphries and Gurney, 2008; Humphries et al, 2006) and small-world measurements (Telesford et al, 2011), to evaluate the small-worldness of the sparse temporal networks. For evaluation based on the small-world coefficient, we compared the clustering coefficient and characteristic path length of each sparse temporal network to the same metrics from equivalent random networks. The small-world coefficient (σ) is defined as (Humphries and Gurney, 2008; Humphries et al, 2006)

$$\sigma=\frac{C/C_{\text{rand}}}{L/L_{\text{rand}}}=\frac{\gamma}{\lambda}, \quad (6)$$

where C and L denote the clustering coefficient and characteristic path length of a sparse temporal network, and C_{rand} and L_{rand} denote the clustering coefficient and characteristic path length of equivalent random networks, and γ and λ denote the normalized clustering coefficient and normalized characteristic path length, respectively. The absolute clustering coefficient for a network G is defined as

$$C=\frac{1}{N}\sum_{i\in G}C_i, \quad (7)$$

where $C_i=\frac{2E_i}{d_i(d_i-1)}$ is the ratio of the number of existing connections to the number of all possible connections, E_i is the number of edges, and d_i is the number of nodes that are directly connected to i-th node with an edge in a subnetwork G_i.

The characteristic path length, which measures the overall routing efficiency, of a network G is defined as the average of the shortest absolute path lengths between the nodes

$$L=\frac{1}{N(N-1)}\sum_{i\in G}\sum_{j\neq i\in G}\min\{L_{i,j}\}, \quad (8)$$

where $\min\{L_{i,j}\}$ denotes the shortest minimum path length between the i-th node and the j-th node. The absolute path length is the number of edges included in the path connecting two nodes. A network is considered as small-world if $C \gg C_{rand}$ and $L \approx L_{rand}$, resulting in $\sigma > 1$.

For evaluation based on the small-world measurement (ω), we compared the clustering coefficient of each sparse temporal network to that of equivalent lattice networks, and compared characteristic path length of each sparse temporal network to that of equivalent random networks (Telesford et al, 2011)

$$\omega=\frac{L_{\text{rand}}}{L}-\frac{C}{C_{\text{latt}}}, \quad (9)$$

where C_{latt} denotes the clustering coefficient of a lattice network. The value of ωis restricted to the interval [−1 1], and a network is considered small-world if $\omega \approx 0$. Positive value indicates a network with more random characteristics (i.e., $L \approx L_{rand}$, and $C \ll C_{latt}$), while negative value indicates a network with more lattice-like characteristics (i.e., $L \gg L_{rand}$, and $C \approx C_{latt}$). It is worth noting that this metric is independent of network size and is more accurate in quantifying small-worldness of a network compared to the small-world coefficient (Telesford et al, 2011).

2.9 Evaluation Via Leave-One-Out Cross-Validation

In this study, we employed SVM with a simple linear kernel based on the LIBSVM library (Chang and Lin, 2011) to evaluate the discriminative power of the features derived from sparse temporal networks. The optimal SVM models as well as an unbiased estimation of the generalization classification performance were achieved via a nested leave-one-out cross-validation scheme due to limited number of sample size. Specifically, for N total number of subjects involved in the study, one was first left out for testing, and the remaining $N-1$ were used for constructing the optimal SVM model. From these $N-1$ samples, $N-1$ different training subsets were formed by each time leaving one more sample out, i.e., $N-2$ subjects in each training subset. For each training subset, functional connectivity construction, feature extraction and feature selection were performed. The performance of each combination of SVM parameters along with the selected features was evaluated using the second left out subject. The combination that gives the best performance was used to construct the optimal SVM model for future classification. This procedure was repeated $N-1$ times, once for each training subset. When the completely unseen test sample was to be classified, all $N-1$ classifiers were used, and the final classification decision was determined via majority voting. This process was repeated N times, each time leaving out a different subject, finally leading to an overall cross-validation classification accuracy. In this study, the optimal λ values for all lasso-based methods were determined via grid search.

3 Experimental Results

3.1 Temporal Network Analysis

Figures 3 and 4 show the small-world coefficient and small-world measurement, respectively, of temporal networks with $N = 90$ and $s = 2$ for the eMCI and the NC groups with respect to random and lattice networks of equivalent distribution. The values $\sigma > 1$ and $\omega \approx 0.3$ (Telesford et al, 2011), indicate the small-worldness of the temporal networks. The small-world coefficients in the eMCI group are smaller than the NC group and show different dynamic patterns across temporal networks (Figure 3). On the other hand, the eMCI group shows larger small-world measurement across temporal networks than the NC group (0.31 *vs.* 0.30). However, different from small-world coefficient, both the eMCI and NC groups do not demonstrate any dynamic pattern across temporal networks in terms of small-world measurement (Figure 4).

To further analyze network properties, we computed the clustering coefficients and characteristic path lengths, and their normalized counterparts, for every temporal network in both groups. The results are shown in Figures 5, 6, 7, 8, respectively, for the temporal networks with $N = 90$ and $s = 2$.We observed distinct dynamic patterns for the eMCI and NC groups in terms of clustering coefficient and its normalized counterpart when BOLD signals were studied at a smaller time scale. Specifically, clustering coefficients for the eMCI group are smaller than NC groups for the first eleven temporal networks, and are larger for the subsequent networks, except for the thirteenth network. On the other hand, the normalized clustering coefficient also showed dynamic pattern but with consistently smaller values in the eMCI group than in the NC group. However, we cannot observe any dynamic pattern for characteristic path length and its normalized counterpart. Characteristic path length is consistently larger in the eMCI group compared with the NC group whereas its normalized counterpart showed an opposite trend with smaller values in the eMCI group. Accordingly to these observations, we have decided to only extract the local clustering coefficient from the temporal networks as our features for constructing SVM classifiers in this study.

3.2 Classification Performance

We compared the eMCI identification performance of the proposed framework with the conventional temporally stationary-based (i.e., Partial correlation (PAC) and Pearson correlation-based (PEC)) methods, sparse inverse covariance matrix (SICE), and the graph graphical LASSO (GGL). For PAC and PEC, entire R-fMRI time series is used to compute one connectivity network. For the SICE and GGL approaches, a series of temporal networks are constructed using ℓ_1 and $\ell_1 + \ell_{2,1}$ penalizations, respectively. Performances of the comparison methods are summarized in Table 1.

The proposed framework performed the best by yielding an accuracy of 79.7%, which is at least 6.5% improvement compared to the second best GGL-based frame-work. The conventional PAC-and PEC-based frameworks performed the worst with classification accuracies of 62.7% and 66.1%, respectively. The proposed, GGL-, and SICE-based frameworks showed a significantly higher sensitivity value when compared to PAC-and PEC-based frameworks. A cross-validation estimation of the generalization performance

shows an area of 0.792 under the receiver operating characteristic curve (AUC), indicating good diagnostic power of the proposed framework.

3.3 Robustness of the Proposed Framework

In the proposed framework, there are two factors that may influence the network topology and correlation strengths of the estimated sparse temporal networks, i.e., sliding window length (N) and translation step size (s), finally the classification performance. To evaluate the robustness of the proposed framework with respect to these two parameters, we repeated eMCI identification using different window lengths (N = 50, 70, 90, 110) and step sizes (s = 1, 2, 4, 8, 10), and their results are summarized in Figure 9. The proposed framework preformed relatively consistent with respect to the window length and step size. When large N and s are used, the proposed framework performed similarly to the conventional PAC-and PEC-based frame-works.

3.4 Most Discriminative Regions

Brain regions that were selected with the highest frequency during the feature selection step based on the training subjects are considered as the most discriminative regions for eMCI identification. These regions (for N = 90 and s = 2) are mostly the components of the Default Mode Network (DMN), i.e., middle frontal gyrus, bilateral superior orbitofrontal cortex, posterior cingulate gyrus, precuneus, and hippocampus. Other selected regions include the frontal lobe (superior frontal gyrus (dorsal) and inferior orbitofrontal cortex), the temporal lobe (superior temporal pole and inferior temporal), the occipital lobe (inferior occipital gyrus, cuneus and bilateral fusiform gyrus), parietal lobe (postcentral gyrus), subcortical regions (caudate and amygdala), and the cerebellum regions (lobule IV, V of cerebellar hemisphere, Lobule VI of cerebellar hemisphere, and lobule X of cerebellar hemisphere (flocculus)). These selected regions are shown in Figure 10. Note that many regions across the brain have been selected for good classification accuracy, particularly the cerebellum regions which are seldom detected in previous studies. For the case of the fully-connected, stationary-based Pearson correlation method, the selected regions include parahippocampus, fusiform gyrus, olfactory, superior frontal gyrus (dorsal), inferior temporal, middle frontal gyrus, and temporal pole (middle). All these regions were selected by our method, although some of them, namely parahippocampus, olfactory, and temporal pole (middle), were chosen with relatively low selection frequency.

4 Discussion

We propose a novel framework that utilizes the temporally dynamic information embraced within an R-fMRI scan to improve disease identification performance. Sparse temporal networks are constructed from the R-fMRI time series, and graph theoretical analysis has been performed to explore their network properties. Clustering coefficient, which shows different dynamic patterns between two clinical groups across sparse temporal networks, was then used to train a linear SVM classifier. Performance of the proposed framework was evaluated on 59 subjects obtained from the ADNI 2 dataset, demonstrating the great importance of including temporally dynamic information for better characterization of brain

activity patterns when compared to the conventional approaches that are based on the temporal stationary assumption.

4.1 Temporal Networks Analysis

The human brain is a complex and highly connected dynamic system with various important topological properties for its optimal functioning (Bullmore and Sporns, 2009; He and Evans, 2010; Rubinov and Sporns, 2010; Stam, 2010). In the brain, clustered regions favor modular information processing; however, several regions in different clusters may have long-range connections that support efficient functional routing (Watts and Strogatz, 1998). Optimal brain networks, which show small-worldness property, are normally characterized by high clustering coefficients like regular lattices, yet low characteristic path lengths like randomly generated networks (Watts and Strogatz, 1998).

Unlike conventional stationary correlation analysis, which generates only one connectivity network per R-fMRI scan, sliding window correlations at different time scales exhibits temporal variations during the R-fMRI scanning session (Allen et al, 2014; Chang and Glover, 2010; Handwerker et al, 2012; Hutchison et al, 2013a; Smith et al, 2012), implying constant activations of the brain even at rest. However, it remains unanswered whether 1) the generated temporal networks are biophysiologically meaningful and exhibit small-world properties as actual human brain networks, 2) there is any between-group difference in terms of temporal network properties, and 3) the differences, if any, can be employed to distinguish eMCI patients from NCs. Therefore, we evaluated the small-world property of the sparse temporal networks by computing the small-world coefficient and the small-world measurement. Consistently large small-world coefficients and close to 0.3 small-world measurements, for both eMCI and NC groups, demonstrate the reliability of the proposed method in generating networks with properties similar to actual brain networks (Telesford et al, 2011). It is worth noting that smaller small-world coefficients and larger small-world measurements indicate that functional connectivity networks in the MCI group are more random compared with the NC group, a common characteristic of most neurodegenerative disorders.

In addition, we observed different dynamic patterns for eMCI and healthy brains in the clustering coefficient and its normalized counterpart. The variations are more obvious in the original clustering coefficient compared to its normalized counterpart. Smooth yet different dynamic patterns in the eMCI and NC groups indicates that 1) changing of brain activity is relatively smooth when the sliding window approach is used due to the overlapping of the R-fMRI time frames, and 2) different dynamic patterns for the eMCI and NC groups can potentially be used as effective biomarkers to identify eMCI patients at individual level. Consistently smaller normalized clustering coefficients are observed in the eMCI group compared with NC group, in line with previous R-fMRI studies (Binnewijzend et al, 2012; Han et al, 2012a; Supekar et al, 2008), although the findings in these studies were obtained based on the conventional stationary assumption.

Temporal networks of the eMCI group showed larger characteristic path length when compared with the NC group, although an opposite trend was observed for its normalized counterpart. Theoretically, a short path length ensures the effective integrity and rapid

information propagation between and across distinct regions of the brain that are believed to constitute the basis of cognitive processing (Sporns and Zwi, 2004). Since neurodegenerative diseases such as AD and MCI are considered to be disconnection syndromes (Delbeuck et al, 2003), larger characteristic path length reflects disrupted neuronal integration between distant regions, in line with previous R-fMRI reports, which show relatively spare long-distant and relatively dense shortdistant functional connections in MCI and AD groups (Buldú et al, 2011; Liu et al, 2012; Seo et al, 2013; Sorg et al, 2007; Wang et al, 2007). Progression of clinical stages, from mild to severe, may cause more impairment or disconnection of longdistant connections, and thus possibly encourage the establishment of short-distant connections within cluster as alternative paths to preserve information transmission between two distant regions. However, establishment of short-distant connections may introduce abnormal clusters that increases the risk of generating an uncontrolled or random flow of information through the entire network (Kaiser, 2007; Kaiser and Hilgetag, 2006; Sanz-Arigita et al, 2010). The decrease in normalized clustering coefficient and characteristic path length, is also reflected by the larger small-world measurement in the eMCI group, suggesting a more random-like network topology.

4.2 Interpretation of Classification Results

Compared with the research (Greicius et al, 2004; Rombouts et al, 2005; Wang et al, 2007) that focuses on group-wise differences, to the best of our knowledge, the current work is the first study that uses temporal dynamics of an R-fMRI scan for disease identification. Although group-wise analysis may identify network changes associated with disease, it is of limited utility at an individual level. In contrast, our goal is to develop an individual-based framework that utilizes the temporal dynamics extracted using one well-known network measure, i.e., clustering coefficients, for disease identification. Promising results using leave-one-out cross-validation indicate the superiority of the proposed temporal network-based framework in eMCI identification when compared with the PAC-, PEC-, SICE, and GGL-based frameworks. Also, the proposed and GGL-based frameworks, both of which include temporally dynamic information, performed better than all other methods, indicating the importance of using temporally dynamic patterns for disease classification, at least in the context of a typical R-fMRI scanning session lasting 5 to 10 minutes.

It has been suggested that correlation values within and between connectivity networks stabilize within 4 ~ 5 minutes of fMRI data (Van Dijk et al, 2010), implying that most studies are adequately sampling the network activity despite relatively few data points, even under variety of behavioral states (e.g., eyes closed, open, or open and fixating) during R-fMRI acquisition. Several studies (Greicius, 2008; Menon, 2011) demonstrated subtle yet significant functional connectivity differences between normal and diseased individuals within similar scanning duration. These findings support, to some extent, our findings where the proposed framework always performs better when sliding window length range is around 3.5 minutes ($N = 70$) and 4.5 minutes ($N = 90$), and with relatively smaller step size (s). The proposed framework performs slightly inferior when the window length (N) and step size (s) are relatively large. With large N and s, it is possible that neural activity changes that occur at time scales shorter than the window length and/or step size are overlooked, causing the performance of the proposed framework approaching to the conventional stationary-based

approaches. This situation is particularly obvious when the window length is similar to the length of entire R-fMRI scan ($M = 130$ in this study). These findings may imply that individuals who are affected by the disease may experience temporal changes, which might be overlooked by the conventional stationary-based approaches.

4.3 Most Discriminative Regions

All the regions that were selected by the conventional fully-connected, stationary-based PC method were also selected by our method as discriminative regions, although with varying selection frequency. More precisely, we observed three different conditions for region selection: a) Selection by the PC method and with relatively high frequency by our method, which indicates a region has informative stationary features; b) Selection by the PC method but with relatively low frequency by our method, which indicates a region's stationary and dynamic features are less informative; and c) Selection with high frequency by our method, without selection by the PC method. In the last case, the dynamic features derived from selected regions greatly contribute to achieving high eMCI identification accuracy. These observations suggest that dynamic patterns of brain regions, which are distributed across sparse temporal networks, provide novel features for detecting possible functional connectivity abnormalities in eMCI patients within an R-fMRI scan. The phenomena of identifying new network nodes (brain regions) that were unobserved at full time series has been reported in anesthetized macaques and awake humans study at shorter window lengths (Hutchison et al, 2013b).

DMN components, which are selected as the most discriminative regions in eMCI identification, exhibit high correlation with the regions in the higher-level cognitive functional networks (e.g., temporo-parietal cortex, inferior frontal cortex, anterior cingulate, and orbital fronto-insular cortices) (Corbetta and Shulman, 2002; Damoiseaux et al, 2006; Seeley et al, 2007). Posterior cingulate cortex, an important component of DMN, demonstrates reduced functional connectivity with the or-bitofrontal cortices and middle frontal gyrus, while increased connectivity with the inferior frontal, fusiform, and precentral regions (Han et al, 2012a) in MCI patients. In addition, MCI patients experience reduced activation compared to NCs in several regions of the occipito-temporal cortex, a small portion of the left inferior frontal gyrus, while increased activation in bilateral anterior cingulate and precueus, with the largest activation differences centered on the fusiform gyri (Gold et al, 2010). Similar fMRI connectivity disruptions have been observed in the posterior hippocampal, and parahippocampal (Hämäläinen et al, 2007). Also, correlation between precuneus and DMN regions has been previously used to distinguish MCI patients from NCs, achieving relatively good accuracy (Rombouts et al, 2005). In our previous R-fMRI study, orbitofrontal cortex, temporal pole, posterior cingulate gyrus, precuneus, and amygdala have been selected as important regions for accurate MCI identification (Wee et al, 2012a). All these findings, either obtained at task-based or task-free fMRI analysis, demonstrate widespread of functional connectivity disruptions across MCI brains even at its prodromal phase (Fennema-Notestine et al, 2009).

Parts of the cerebellum regions of MCI patients underwent structural degenerative (Baloyannis et al, 2000; Fukutani et al, 1997; Li et al, 1994; Sjöbeck and Englund, 2001;

Wang et al, 2002), including reduction of Purkinje cell density, atrophy of the molecular and granular cell layer, and concentration of amyloid plaques in the cerebellar cortex (Wegiel et al, 1999). In a study that manually partitioned human cerebellum into four substructures, i.e., anterior, superior posterior, inferior posterior lobes, and corpus medullare on each hemisphere, the posterior cerebellar lobe experience significant volume reduction in AD patients (Thomann et al, 2008), leading to poorer cognitive performance. In terms of functional study, the left cerebellum is activated in memory encoding task (Kircher et al, 2007), implying its association with recognition memory. Another event-related study suggested that the cerebellar regions contribute to human recognition (Weis et al, 2004). Compared to the structural and task-based functional studies, the cerebellum regions were always been ignored in the R-fMRI-based AD/MCI analysis. Our findings of detecting cerebellum regions as the important features for accurate eMCI identification may suggest the disruption of cerebellum functions in AD/MCI brains, thus merit for more attention in the future R-fMRI-based AD/MCI study.

4.4 Methodological Issues/Limitations

The current study has three main limitations. First, the proposed framework is based on the temporal dynamics in the R-fMRI scan, however, neurobiological underpinnings and mechanisms of these temporal dynamics are still largely unknown (Smith et al, 2011). It is possible that sliding window correlation variations in the sparse temporal networks are associated with changes in brain state or arousal. However, we cannot rule out the possibility that these changes are driven simply by the noise (e.g. motion, physiological, and scanner noises) (Handwerker et al, 2012). Hence, careful interpretations of the results are required, and more works shall be performed to improve our understanding on these issues.

Second, the choice of window size is important for the sliding window approach. The window length should be long enough to permit robust estimation of functional connectivity and short enough to allow the detection of interesting short-term fluctuations (Saköglu et al, 2010). As the window shrinks, the signal-to-noise ratio decreases since there are fewer time points available for connectivity estimation. The estimation variability may increase due to signals of higher frequencies, physiological noise, and head motion (Hutchison et al, 2013a). On the other hand, as the window expands, brief neural activities tend to be smoothed out. Since brain activation patterns vary with diseases, it is therefore important to vary the window size to capture brain activities of different time scales.

Third, the diagnosis criteria of eMCI are still unclear and standard where they may be similar to the early diagnosis of other neurodegenerative dementia such Parkinson disease and frontotemporal dementia. This may rise reliability issue of the eMCI diagnosis. Third, subjects used in this study are at the very beginning stage of AD and there are very few studies focused in this type of cohort. Due to this, the selected most discriminative regions can only be compared with the AD/MCI findings using the conventional stationary approach. However, these selected brain regions spread over the whole brain, thus future analysis is required to verify these findings.

5 Conclusions

In this paper, we propose to utilize the temporally dynamic information of an R-fMRI scan for disease identification. This work is motivated by the variabilities of sliding window correlation strengths induced by the neural interactions that happen within time scales that are shorter than a typical R-fMRI scanning session. Unlike the conventional approach that assumes functional connectivity is temporally stationary, we estimate temporal networks from a set of R-fMRI sub-series using a sliding window approach to extract the between-region neural interactions across time. We utilize a fused LASSO regularization-based sparse learning algorithm to jointly estimate temporal networks, encouraging similar network topology and correlation strengths between temporally adjoining networks. Clustering coefficients are calculated from each network to extract temporally dynamic patterns. Promising results on eMCI identification suggest that the temporal dynamic information encapsulated in an R-fMRI scan is crucial for accurate diagnosis of neurological disorders. In the future, we will extend the proposed disease identification framework for diagnosis of neurodevelopmental disorders such as autism and attention deficit hyperactivity disorder (ADHD), which can benefit greatly from early detection.

Acknowledgments

This work was supported in part by NIH grants AG041721, AG042599, EB008374, EB009634, and MH100217.

Data collection and sharing for this project was funded by the Alzheimer's Disease Neuroimaging Initiative (ADNI) (National Institutes of Health Grant U01 AG024904). ADNI is funded by the National Institute on Aging, the National Institute of Biomedical Imaging and Bioengineering, and through generous contributions from the following: Abbott; Alzheimer's Association; Alzheimer's Drug Discovery Foundation; Amorfix Life Sciences Ltd.; AstraZeneca; Bayer HealthCare; BioClinica, Inc.; Biogen Idec Inc.; Bristol-Myers Squibb Company; Eisai Inc.; Elan Pharmaceuticals Inc.; Eli Lilly and Company; F. Hoffmann-La Roche Ltd and its affiliated company Genentech, Inc.; GE Healthcare; Innogenetics, N.V.; Janssen Alzheimer Immunotherapy Research & Development, LLC.; Johnson & Johnson Pharmaceutical Research & Development LLC.; Medpace, Inc.; Merck & Co., Inc.; Meso Scale Diagnostics, LLC.; Novartis Pharmaceuticals Corporation; Pfizer Inc.; Servier; Synarc Inc.; and Takeda Pharmaceutical Company. The Canadian Institutes of Health Research is providing funds to support ADNI clinical sites in Canada. Private sector contributions are facilitated by the Foundation for the National Institutes of Health (www.fnih.org). The grantee organization is the Northern California Institute for Research and Education, and the study is coordinated by the Alzheimer's Disease Cooperative Study at the University of California, San Diego. ADNI data are disseminated by the Laboratory for Neuro Imaging at the University of California, Los Angeles. This research was also supported by NIH grants P30 AG010129, K01 AG030514, and the Dana Foundation.

Appendix A. The Alzheimer's Disease Neuroimaging Initiative (ADNI)

The ADNI was launched in 2003 by the National Institute on Aging (NIA), the National Institute of Biomedical Imaging and Bioengineering (NIBIB), the Food and Drug Administration (FDA), private pharmaceutical companies and non-profit organizations, as a $60 million as a landmark study that gathered and analyzed thousands of brain scans, genetic profiles and biomarkers in blood and cerebrospinal fluid (CSF). Although the original goal was to define biomarkers for use in clinical trials to determine the best way to measure treatment effects of AD, the goal has been expanded to find more sensitive and accurate methods to detect AD at a pre-dementia stage and mark its progress through biomarkers. ADNI 1 involves scientists at 59 research centers, 54 in USA and 5 in Canada. The Principal Investigator of this initiative is Dr. Michael W. Weiner, MD, VA Medical Center and University of California, San Francisco. Originally 800 participants were

enrolled, which comprised of 200 with AD patients, 400 with MCI and 200 with normal cognition. In 2010, the ADNI study moved into the ADNI GO[3] phase to focus on participants who exhibit the earliest signs of memory loss in MCI. While the ADNI GO project work continues, the overall ADNI effort is rapidly moving into a third phase, i.e., ADNI 2[4]. ADNI 2 will build upon the successes of earlier ADNI phases to identify the earliest signs of AD. Researchers are eager to determine when damage to the brain begins. The ADNI 2 phase of the study includes a large number of new volunteers in the earliest stages of cognitive impairment.

References

Achard S, Bullmore E. Efficiency and cost of economical brain functional networks. PLoS Comput Biol. 2007; 3(2):e17. [PubMed: 17274684]

Achard S, Salvador R, Whitcher B, Suckling J, Bullmore ET. A resilient, low-frequency, small-world human brain functional network with highly connected association cortical hubs. J Neurosci. 2006; 26(1):63–72. [PubMed: 16399673]

Allen EA, Damaraju E, Plis SM, Erhardt EB, Eichele T, Calhoun VD. Tracking whole-brain connectivity dynamics in the resting state. Cereb Cortex. 2014; 24(3):663–676. [PubMed: 23146964]

Baloyannis S, Manolidis S, Manolidis L. Synaptic alterations in the vestibulocerebellar system in alzheimer's disease - a golgi and electron microscope study. Acta Otolaryngol. 2000; 120(2):247–250. [PubMed: 11603783]

Binnewijzend MA, Schoonheim MM, Sanz-Arigita E, Wink AM, van der Flier WM, Tolboom N, Adriaanse SM, Damoiseaux JS, Scheltens P, van Berckel BN, Barkhof F. Resting-state fMRI changes in Alzheimer's disease and mild cognitive impairment. Neurobiol Aging. 2012; 33(9): 2018–2028. [PubMed: 21862179]

Buldú JM, Bajo R, Maestú F, Castellanos N, Leyva I, Gil P, na Nadal IS, Almendral JA, Nevado A, del Pozo F, Boccaletti S. Reorganization of functional networks in mild cognitive impairment. PLoS ONE. 2011; 6(5):e19,584.

Bullmore E, Sporns O. Complex brain networks: Graph theoretical analysis of structural and functional systems. Nat Rev Neurosci. 2009; 10:186–198. [PubMed: 19190637]

Chang C, Glover GH. Time-frequency dynamics of resting-state brain connectivity measured with fMRI. Neuroimage. 2010; 50(1):81–98. [PubMed: 20006716]

Chang C, Liu Z, Chen MC, Liu X, Duyn JH. EEG correlates of time-varying BOLD functional connectivity. Neuroimage. 2013; 72:227–236. in Press. [PubMed: 23376790]

Chang CC, Lin CJ. LIBSVM: A library for support vector machines. ACM TIST. 2011; 2(3):27, 1–27. software available at http://www.csie.ntu.edu.tw/cjlin/libsvm.

Chen, X.; He, J.; Lawrence, R.; Carbonell, J. Adaptive multi-task sparse learning with an application to fMRI study. SIAM International Conference on Data Mining (SDM), SIAM; California, USA. 2012. p. 212-223.

Corbetta M, Shulman GL. Control of goal-directed and stimulus-driven attention in the brain. Nat Rev Neurosci. 2002; 3(3):201–215. [PubMed: 11994752]

Damoiseaux JS, Rombouts SARB, Barkhof F, Scheltens P, Stam CJ, Smith SM, Beckmann CF. Consistent resting-state networks across healthy subjects. Proc Natl Acad Sci U S A. 2006; 103(37):13,848–13,853.

Danaher P, Wang P, Witten DM. The joint graphical lasso for inverse covariance estimation across multiple classes. 2012 Arxiv preprint arXiv:1111.0324.

Delbeuck X, Van der Linden M, Collette F. Alzheimer's disease as a disconnection syndrome? Neuropsychol Rev. 2003; 13(2):79–92. [PubMed: 12887040]

[3] http://www.adcs.org/studies/imagineadni.aspx
[4] http://adcs.org/studies/ImagineADNI2.aspx

Dosenbach NUF, Fair DA, Miezin FM, Cohen AL, Wenger KK, Dosenbach RAT, Fox MD, Snyder AZ, Vincent JL, Raichle ME, Schlaggar BL, Petersen SE. Distinct brain networks for adaptive and stable task control in humans. Proc Natl Acad Sci U S A. 2007; 104(26):11,073–11,078.

Dubois B, Albert ML. Amnestic MCI or prodromal Alzheimer's disease? Lancet Neurol. 2004; 3(4): 246–248. [PubMed: 15039037]

Economou A, Papageorgiou SG, Karageorgiou C, Vassilopoulos D. Nonepisodic memory deficits in amnestic MCI. Cogn Behav Neurol. 2007; 20(2):99–106. [PubMed: 17558253]

Fennema-Notestine C, Hagler DJ Jr, McEvoy LK, Fleisher AS, Wu EH, Karow DS, Dale AM. Alzheimer's Disease Neuroimaging Initiative. Structural MRI biomarkers for preclinical and mild Alzheimer's disease. Hum Brain Mapp. 2009; 30(10):3238–3253. [PubMed: 19277975]

Fox MD, Zhang D, Snyder AZ, Raichle ME. The global signal and observed anticorrelated resting state brain networks. J Neurophysiol. 2009; 101(6):3270–3283. [PubMed: 19339462]

Fransson P, Marrelec G. The precuneus/posterior cingulate cortex plays a pivotal role in the default mode network: Evidence from a partial correlation network analysis. Neuroimage. 2008; 42:1178–1184. [PubMed: 18598773]

Friedman J, Hastie T, Tibshirani R. Sparse inverse covariance estimation with the graphical lasso. Biostatistics. 2008; 9(3):432–441. [PubMed: 18079126]

Fukutani Y, Cairns NJ, Rossor MN, Lantos PL. Cerebellar pathology in sporadic and familial Alzheimer's disease including APP 717 (Val→Ile) mutation cases: a morphometric investigation. J Neurol Sci. 1997; 149(2):177–184. [PubMed: 9171327]

Gold BT, Jiang Y, Jicha GA, Smith CD. Functional response in ventral temporal cortex differentiates mild cognitive impairment from normal aging. Hum Brain Mapp. 2010; 31(8):1249–1259. [PubMed: 20063353]

Greicius M. Resting-state functional connectivity in neuropsychiatric disorders. Curr Opin Neurol. 2008; 21:424–430. [PubMed: 18607202]

Greicius MD, Srivastava G, Reiss AL, Menon V. Default-mode network activity distinguishes alzheimer's disease from healthy aging: evidence from functional mri. Proc Natl Acad Sci U S A. 2004; 101(13):4637–4642. [PubMed: 15070770]

Hämäläinen A, Pihlajamäki M, Tanila H, Hänninen T, Niskanen E, Tervo S, Karjalainen PA, Vanninen RL, Soininen H. Increased fMRI responses during encoding in mild cognitive impairment. Neurobiol Aging. 2007; 28(12):1889–1903. [PubMed: 16997428]

Han SD, Arfanakis K, Fleischman DA, Leurgans SE, Tuminello ER, Edmonds EC, Bennett DA. Functional connectivity variations in mild cognitive impairment: Associations with cognitive function. J Int Neuropsychol Soc. 2012a; 18(1):39–48. [PubMed: 22005016]

Han Y, Lui S, Kuang W, Lang Q, Zou L, Jia J. Anatomical and functional deficits in patients with amnestic mild cognitive impairment. PLoS ONE. 2012b; 7(2):e28,664.

Handwerker DA, Roopchansingh V, Gonzalez-Castillo J, Bandettini PA. Periodic changes in fMRI connectivity. Neuroimage. 2012; 63(3):1712–1719. [PubMed: 22796990]

He Y, Evans A. Graph theoretical modeling of brain connectivity. Curr Opin Neurol. 2010; 23:341–350. [PubMed: 20581686]

Huang S, Li J, Sun L, Ye J, Fleisher A, Wu T, Chen K, Reiman E. Learning brain connectivity of Alzheimer's disease by sparse inverse covariance estimation. Neuroimage. 2010; 50(3):935–949. [PubMed: 20079441]

Humphries MD, Gurney K. Network 'small-world-ness': A quantitative method for determining canonical network equivalence. PLoS ONE. 2008; 3(4):e0002,051.

Humphries MD, Gurney K, Prescott TJ. The brainstem reticular formation is a small-world, not scale-free, network. Proc Biol Sci. 2006; 273(1585):503–511. [PubMed: 16615219]

Hutchison RM, Womelsdorf T, Allen EA, Bandettini PA, Calhoun VD, Corbetta M, Penna SD, Duyn JH, Glover GH, Gonzalez-Castillo J, Handwerker DA, Keilholz S, Kiviniemi V, Leopold DA, de Pasquale F, Sporns O, Walter M, Chang C. Dynamic functional connectivity: Promises, issues, and interpretations. Neuroimage. 2013a; 80:360–368. [PubMed: 23707587]

Hutchison RM, Womelsdorf T, Gati JS, Everling S, Menon RS. Resting-state networks show dynamic functional connectivity in awake humans and anesthetized macaques. Hum Brain Mapp. 2013b; 34(9) 2154 –4 2177.

Jia H, Hu X, Deshpande G. Finite number of brain network configurations revealed from time-varying connectivity assessment of resting state fMRI. Proc Intl Soc Mag Reson Med. 2013:0036.

Johnson SC, Schmitz TW, Moritz CH, Meyerand ME, Rowley HA, Alexander AL, Hansen KW, Gleason CE, Carlsson CM, Ries ML, Asthana S, Chen K, Reiman EM, Alexander GE. Activation of brain regions vulnerable to Alzheimer's disease: The effect of mild cognitive impairment. Neurobiol Aging. 2006; 27(11):1604–1612. [PubMed: 16226349]

Jones DT, Vemuri P, Murphy MAC, Gunter JL, Senjem ML, Machulda MM, Przybelski SA, Gregg BE, Kantarci K, Knopman DS, Boeve BF, Petersen RC, Jack CR Jr. Non-stationarity in the "resting brain's" modular architecture. PLoS ONE. 2012; 7:e39,731.

Kaiser M. Brain architecture: a design for natural computation. Philos Trans A Math Phys Eng Sci. 2007; 365(1861):3033–3045. [PubMed: 17855223]

Kaiser M, Hilgetag CC. Nonoptimal component placement, but short processing paths, due to long-distance projections in neural systems. PLoS Comput Biol. 2006; 2(7):e95. [PubMed: 16848638]

Kircher TT, Weis S, Freymann K, Erb M, Jessen F, Grodd W, Heun R, Leube DT. Hippocampal activation in patients with mild cognitive impairment is necessary for successful memory encoding. J Neurol Neurosurg Psychiatry. 2007; 78(8):812–818. [PubMed: 17287238]

Kötter R, Stephen KE. Network participation indices: Characterizing component roles for information processing in neural networks. Neural Netw. 2003; 16(9):1261–1275. [PubMed: 14622883]

Li C, Wang J, Gui L, Zheng J, Liu C, Du H. Alterations of whole-brain cortical area and thickness in mild cognitive impairment and Alzheimer's disease. J Alzheimers Dis. 2011; 27(2):281–290. [PubMed: 21799248]

Li Y, Wang Y, Wu G, Shi F, Zhou L, Lin W, Shen D. Alzheimer's Disease Neuroimaging Initiative. Discriminant analysis of longitudinal cortical thickness changes in alzheimer's disease using dynamic and network features. Neurobiol Aging. 2012; 33(2):427.e15–427.e30. [PubMed: 21272960]

Li YT, Woodruff-Pak DS, Trojanowski JQ. Amyloid plaques in cerebellar cortex and the integrity of Purkinje cell dendrites. Neurobiol Aging. 1994; 15(1):1–9. [PubMed: 8159255]

Liu Z, Zhang Y, Bai L, Yan H, Dai R, Zhong C, Wang H, Wei W, Xue T, Feng Y, You Y, Tian J. Investigation of the effective connectivity of resting state networks in Alzheimer's s disease: A functional MRI study combining independent components analysis and multivariate Granger causality analysis. NMR in Biomedicine. 2012; 25(1):1311–1320. [PubMed: 22505275]

Lynall ME, Bassett DS, Kerwin R, McKenna PJ, Kitzbichler M, Muller U, Bullmore ET. Functional connectivity and brain networks in Schizophrenia. J Neurosci. 2010; 30:9477–9487. [PubMed: 20631176]

McEvoy LK, Fennema-Notestine C, Roddey JC Jr DJH, Holland D, Karow DS, Pung CJ, Brewer JB, Dale AM. Alzheimer disease: Quantitative structural neuroimaging for detection and prediction of clinical and structural changes in mild cognitive impairment. Radiology. 2009; 251:195–205. [PubMed: 19201945]

Menon V. Large-scale brain networks and psychopathology: a unifying triple network model. Trends Cogn Sci. 2011; 15:483–506. [PubMed: 21908230]

Murphy K, Birn RM, Handwerker DA, Jones TB, Bandettini PA. The impact of global signal regression on resting state correlations: are anti-correlated networks introduced? Neuroimage. 2009; 44(3):893–905. [PubMed: 18976716]

Rombouts SARB, Barkhof F, Goekoop R, Stam CJ, Scheltens P. Altered resting state networks in mild cognitive impairment and mild Alzheimer's disease: An fMRI study. Hum Brain Mapp. 2005; 26(4):231–239. [PubMed: 15954139]

Rubinov M, Sporns O. Complex networks measures of brain connectivity: Uses and interpretations. Neuroimage. 2010; 52(3):1059–1069. DOI. [PubMed: 19819337]

Saköglu U, Pearlson GD, Kiehl KA, Wang Y, Michael A, Calhoun VD. A method for evaluating dynamic functional network connectivity and task-modulation: application to schizophrenia. MAGMA. 2010; 23(5–6):351–366. [PubMed: 20162320]

Sanz-Arigita EJ, Schoonheim MM, Damoiseaux JS, Rombouts SARB, Maris E, Barkhof F, Scheltens P, Stam CJ. Loss of 'small-world' networks in alzheimer's disease: Graph analysis of fmri resting-state functional connectivity. PLoS ONE. 2010; 5(11):e13,788.

Seeley WW, Menon V, Schatzberg AF, Keller J, Glover GH, Kenna H, Reiss AL, Greicius MD. Dissociable intrinsic connectivity networks for salience processing and executive control. J Neurosci. 2007; 27(9):2349–2356. [PubMed: 17329432]

Seo EH, Lee DY, Lee JM, Park JS, Sohn BK, Lee DS, Choe YM, Woo JI. Whole-brain functional networks in cognitively normal, mild cognitive impairment, and alzheimer's disease. PLoS ONE. 2013; 8(1):e53,922.

Sheline YI, Raichle ME. Resting state functional connectivity in preclinical alzheimer's disease. Biol Psychiatry. 2013; 74(5):340–347. [PubMed: 23290495]

Sjöbeck M, Englund E. Alzheimer's disease and the cerebellum: A morphologic study on neuronal and glial changes. Dement Geriatr Cogn Disord. 2001; 12(3):211–218. [PubMed: 11244215]

Smith CD, Chebrolu H, Wekstein DR, Schmitt FA, Jicha GA, Cooper G, Markesbery WR. Brain structural alterations before mild cognitive impairment. Neurology. 2007; 68(16):1268–1273. [PubMed: 17438217]

Smith SM, Miller KL, Salimi-Khorshidi G, Webster M, Beckmann CF, Nichols TE, Ramsey JD, Woolrich MW. Network modelling methods for fMRI. Neuroimage. 2011; 54(2):875–891. [PubMed: 20817103]

Smith SM, Miller KL, Moeller S, Xu J, Auerbach EJ, Woolrich MW, Beckmann CF, Jenkinson M, Andersson J, Glasser MF, Van Essen DC, Feinberg DA, Yacoub ES, Ugurbil K. Temporally-independent functional modes of spontaneous brain activity. Proc Natl Acad Sci U S A. 2012; 109(8):3131. [PubMed: 22323591]

Sorg C, Riedl V, Perneczky R, Kurz A, Wohlschlager AM. Selective changes of resting-state networks in individuals at risk for Alzheimer's disease. Proc Natl Acad Sci U S A. 2007; 104(47):18,760–18,765.

Sporns O. The human connectome: A complex network. Ann N Y Acad Sci. 2011; 1224:109–125. [PubMed: 21251014]

Sporns O, Zwi JD. The small world of the cerebral cortex. Neuroinformatics. 2004; 2:145–161. [PubMed: 15319512]

Sporns O, Chialvo DR, Kaiser M, Hilgetag CC. Organization, development and function of complex brain networks. Trends Cogn Sci. 2004; 8(9):418–425. [PubMed: 15350243]

Stam CJ. Characterization of anatomical and functional connectivity in the brain: a complex networks perspective. Int J Psychophysiol. 2010; 77(3):186–194. [PubMed: 20598763]

Stam CJ, Jones BF, Nolte G, Breakspear M, Scheltens P. Small-world networks and functional connectivity in Alzheimer's disease. Cereb Cortex. 2007; 17:92–99. [PubMed: 16452642]

Suk HI, Wee CY, Shen D. Discriminative group sparse representation for mild cognitive impairment classification. Machine Learning in Medical Imaging. 2013:131–138.

Suk HI, Wee CY, Lee SW, Shen D. Suparvised discriminative group sparse representation for mild cognitive impairment diagnosis. Neuroinformatics. 2014 Epub.

Supekar K, Menon V, Rubin D, Musen M, Greicius MD. Network analysis of intrinsic functional brain connectivity in Alzheimer's disease. PLoS Comput Biol. 2008; 4:e1000,100.

Tabert MH, Manly JJ, Liu X, Pelton GH, Rosenblum S, Jacobs M, Zamora D, Goodkind M, Bell K, Stern Y, Devanand DP. Neuropsychological prediction of conversion to alzheimer disease in patients with mild cognitive impairment. Arch Gen Psychiatry. 2006; 63(8):916–924. [PubMed: 16894068]

Telesford QK, Joyce KE, Hayasaka S, Burdette JH, Laurienti PJ. The ubiquity of small-world networks. Brain Connect. 2011; 1(5):367–375. [PubMed: 22432451]

Thomann PA, Schläfer C, Seidl U, Santos VD, Essig M, Schröder J. The cerebellum in mild cognitive impairment and Alzheimer's disease - a structural mri study. J Psychiatr Res. 2008; 42(14):198–202.

Thompson PM, Apostolova LG. Computational anatomical methods as applied to ageing and dementia. Br J Radiol. 2007; 80(2):S78–S91. [PubMed: 18445748]

Tibshirani R, Sauders M, Zhu J, Knight K. Sparsity and smoothness via the fused lasso. J R Statist Soc B. 2005; 67(1):91–108.

Tomasi D, Wang R, Wang GJ, Volkow ND. Functional connectivity and brain activation: A synergistic approach. 2013 in Press.

Tzourio-Mazoyer N, Landeau B, Papathanassiou D, Crivello F, Etard O, Delcroix N, Mazoyer B, Joliot M. Automated anatomical labeling of activations in SPM using a macroscopic anatomical parcellation of the MNI MRI single-subject brain. Neuroimage. 2002; 15:273–289. [PubMed: 11771995]

Van Dijk KRA, Hedden T, Venkataraman A, Evans KC, Lazar SW, Buckner RL. Intrinsic functional connectivity as a tool for human connectomics: Theory, properties and optimization. J Neurophysiol. 2010; 103:297–321. [PubMed: 19889849]

Wang HY, D'Andrea MR, Nagele R. Cerebellar diffuse amyloid plaques are derived from dendritic Abeta42 accumulations in Purkinje cells. Neurobiol Aging. 2002; 23(2):213–223. [PubMed: 11804705]

Wang J, Zuo X, He Y. Graph-based network analysis of resting-state functional MRI. Front Syst Neurosci. 2010; 4:16. [PubMed: 20589099]

Wang K, Liang M, Wang L, Tian L, Zhang X, Li K, Jiang T. Altered functional connectivity in early Alzheimer's disease: A resting-state fMRI study. Hum Brain Mapp. 2007; 28(10):967–978. [PubMed: 17133390]

Watts DJ, Strogatz SH. Collective dynamics of "small-world" networks. Nature. 1998; 393:440–442. [PubMed: 9623998]

Wee CY, Yap PT, Denny K, Browndyke JN, Potter GG, Welsh-Bohmer KA, Wang L, Shen D. Resting-state multi-spectrum functional connectivity networks for identification of MCI patients. PLoS ONE. 2012a; 7(5):e37,828.

Wee CY, Yap PT, Zhang D, Denny K, Browndyke JN, Potter GG, Welsh-Bohmer KA, Wang L, Shen D. Identification of mci individuals using structural and functional connectivity networks. Neuroimage. 2012b; 59(3):2045–2056. [PubMed: 22019883]

Wee CY, Yap PT, Shen D. for the Alzheimer's Disease Neuroimaging Initiative. Prediction of Alzheimer's disease and mild cognitive impairment using cortical morphological patterns. Hum Brain Mapp. 2013; 34(12):3411–3425. [PubMed: 22927119]

Wee CY, Yap PT, Zhang D, Shen D. Group-constrained sparse fmri connectivity modeling for mild cognitive impairment identification. Brain Struct Funct. 2014; 219(2):641–656. [PubMed: 23468090]

Wegiel J, Wisniewski HM, Dziewiatkowski J, Badmajew E, Tarnawski M, Reisberg B, Mlodzik B, Leon MJD, Miller DC. Cerebellar atrophy in alzheimer's disease - clinicopathological correlations. Brain Res. 1999; 818(1):41–50. [PubMed: 9914436]

Weis S, Klaver P, Reul J, Elger CE, Fernández G. Temporal and cerebellar brain regions that support both declarative memory formation and retrieval. Cereb Cortex. 2004; 14(3):256–267. [PubMed: 14754866]

Whitwell JL, Przybelski SA, Weigand SD, Knopman DS, Boeve BF, Petersen RC, Jack CR Jr. 3d maps from multiple mri illustrate changing atrophy patterns as subjects progress from mild cognitive impairment to Alzheimer's disease. Brain. 2007; 130(7):1777–1786. [PubMed: 17533169]

Yang S, Pan Z, Shen X, Wonka P, Ye J. Fused multiple graphical lasso. 2012 Arxiv preprint arXiv: 1209.2139.

Zhang D, Shen D. Alzheimer's Disease Neuroimaging Initiative. Predicting future clinical changes of mci patients using longitudinal and multimodal biomarkers. PLoS ONE. 2012; 7(3):e33,182.

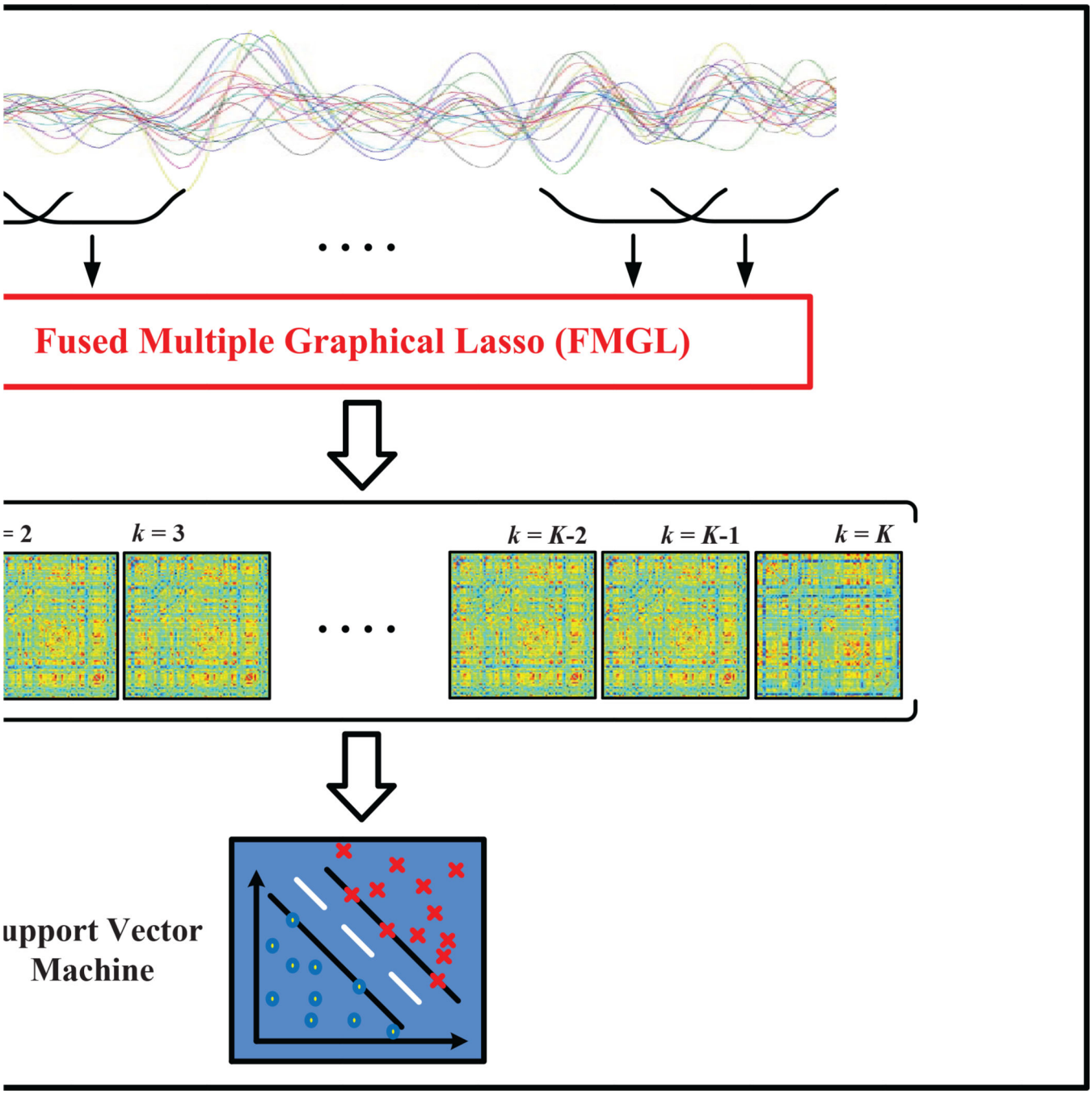

Fig. 1.
The proposed sparse temporal network-based disease identification frame-work.

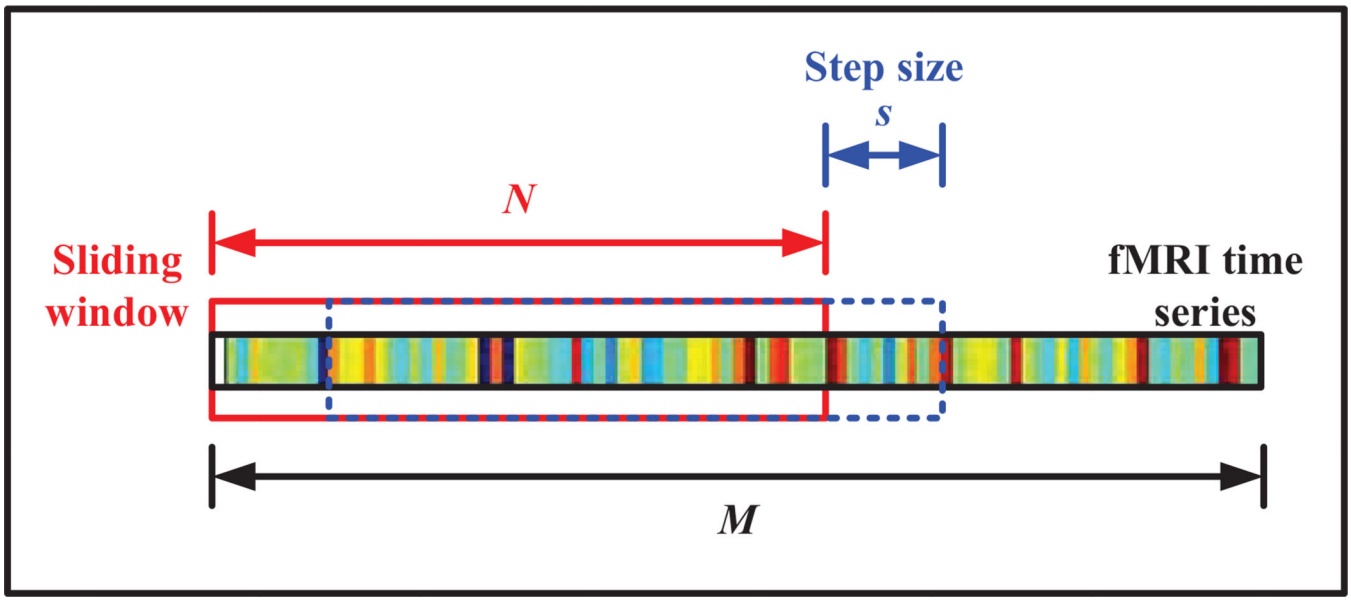

Fig. 2.
Generation of R-fMRI sub-series using sliding window approach.

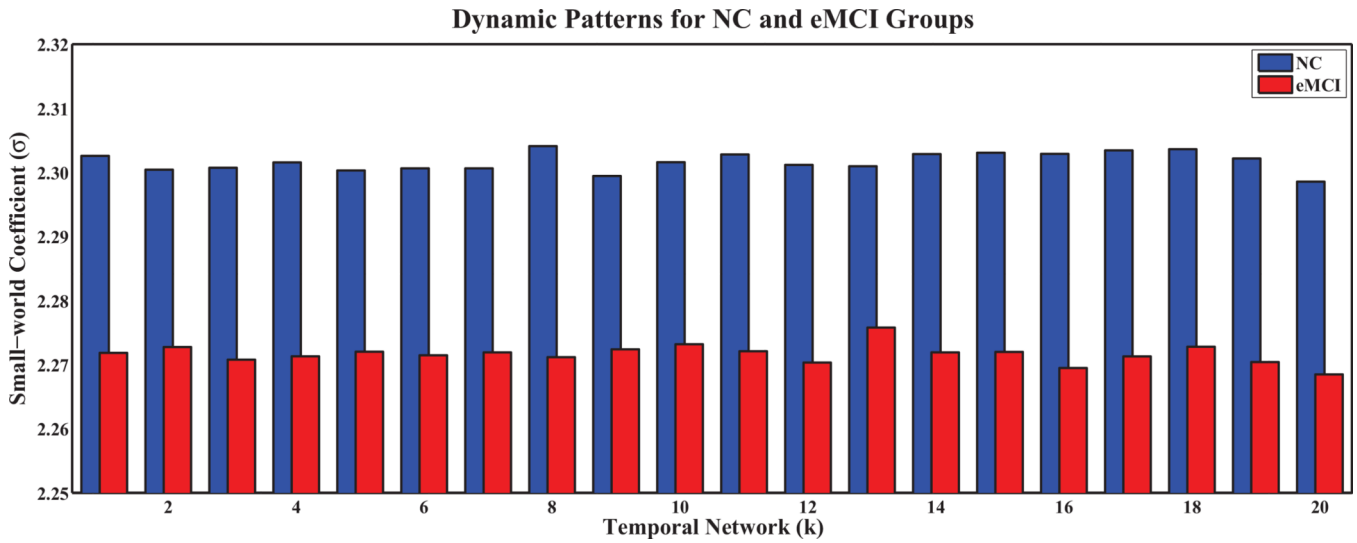

Fig. 3.

Small-world coefficient (σ) of dynamic sparse temporal networks for eMCI and NC groups with respect to random networks.

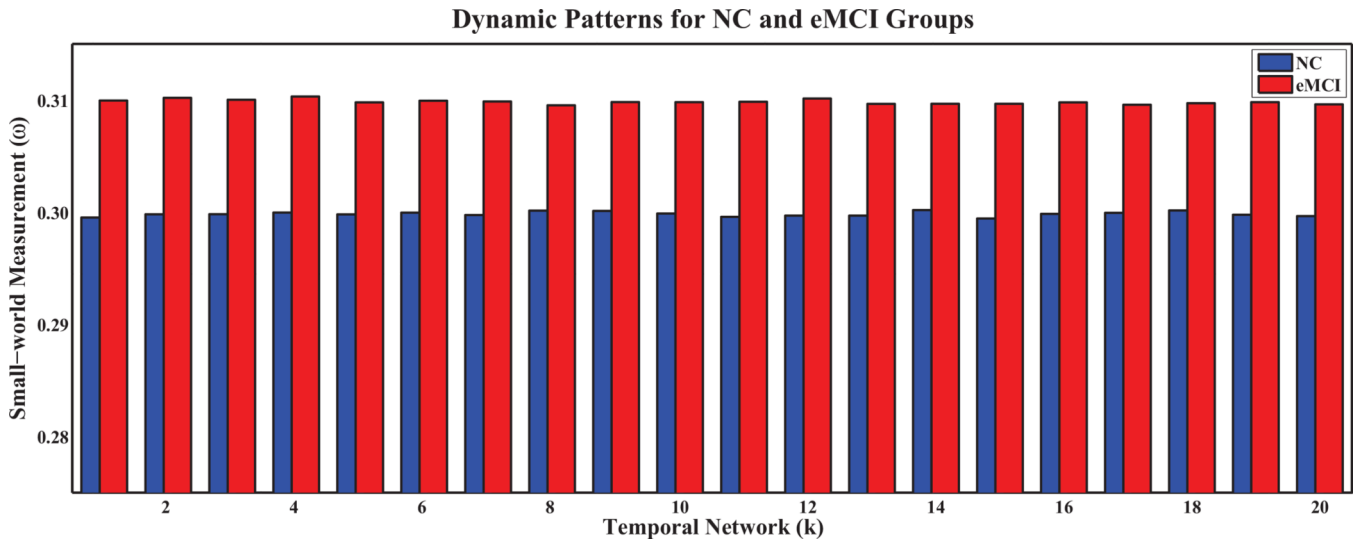

Fig. 4.

Small-world measurement (ω) of dynamic sparse temporal networks for eMCI and NC groups with respect to random and lattice networks.

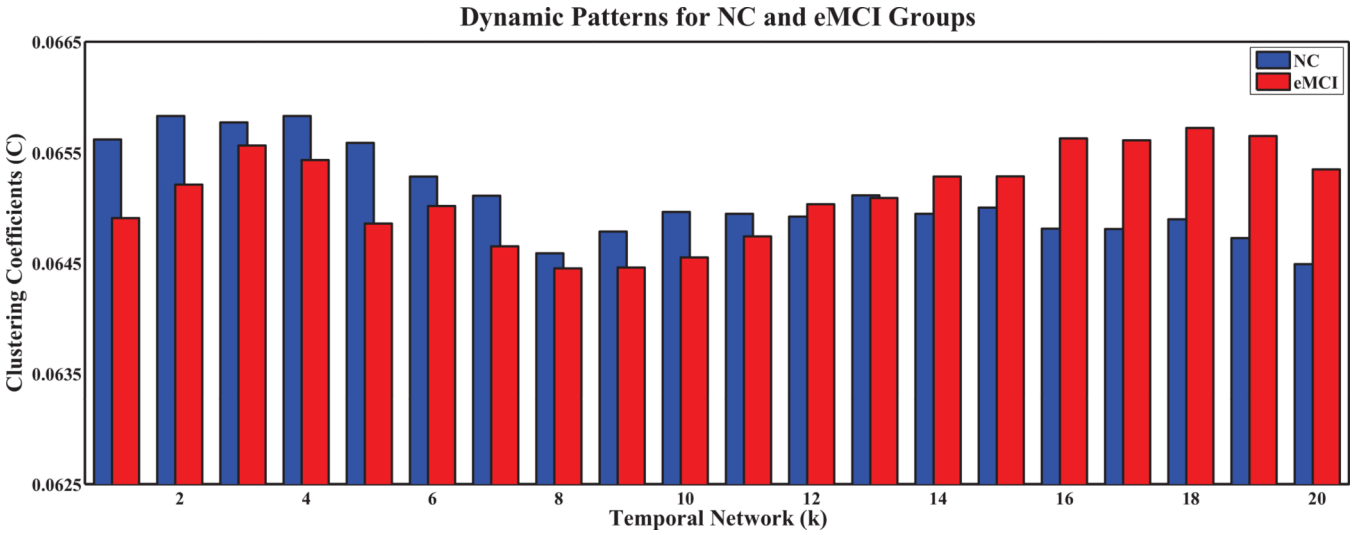

Fig. 5.

Clustering coefficients of temporal networks for eMCI and NC groups with $s = 2$ and $N = 90$.

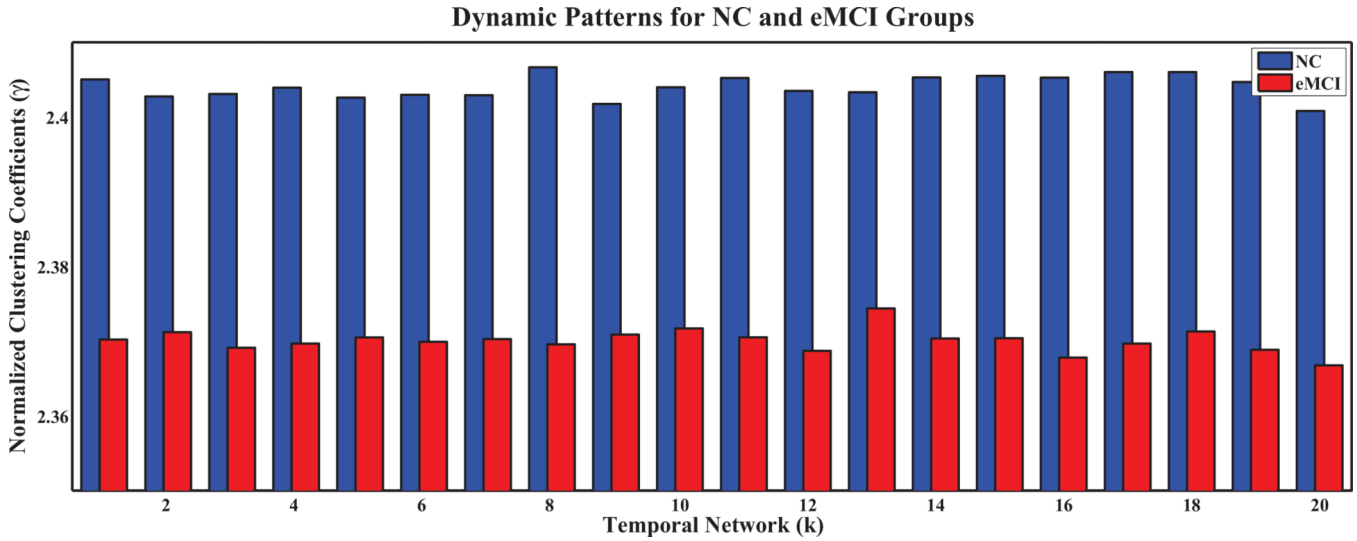

Fig. 6.

Normalized clustering coefficients of temporal networks for eMCI and NC groups with $s = 2$ and $N = 90$.

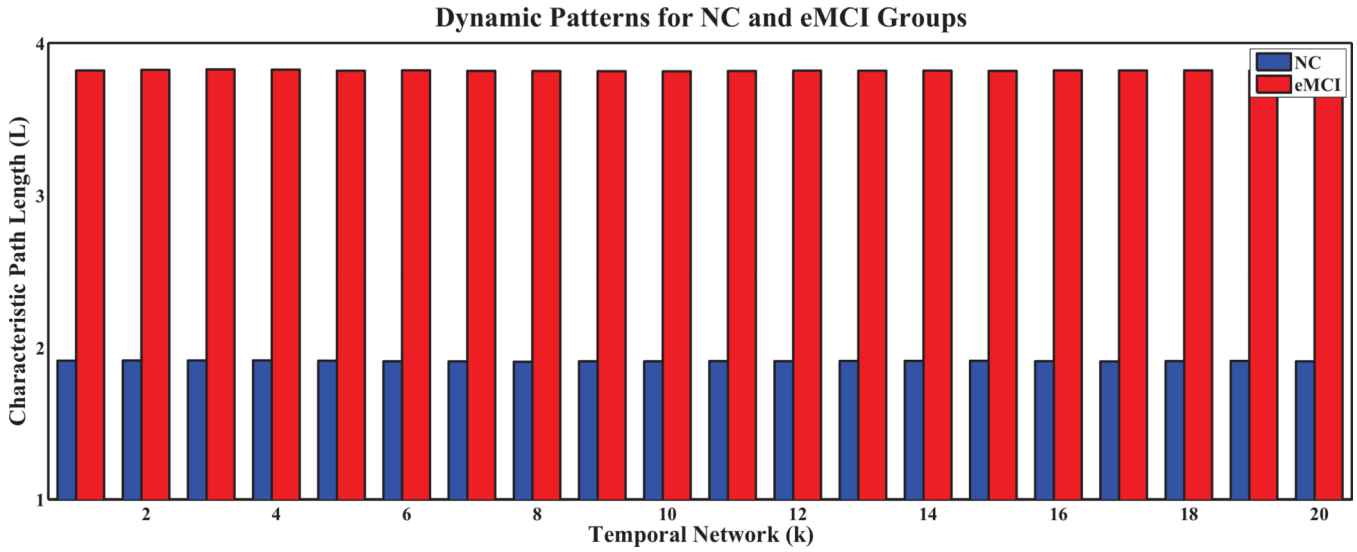

Fig. 7.

Characteristic path lengths of temporal networks for eMCI and NC groups with $s = 2$ and $N = 90$.

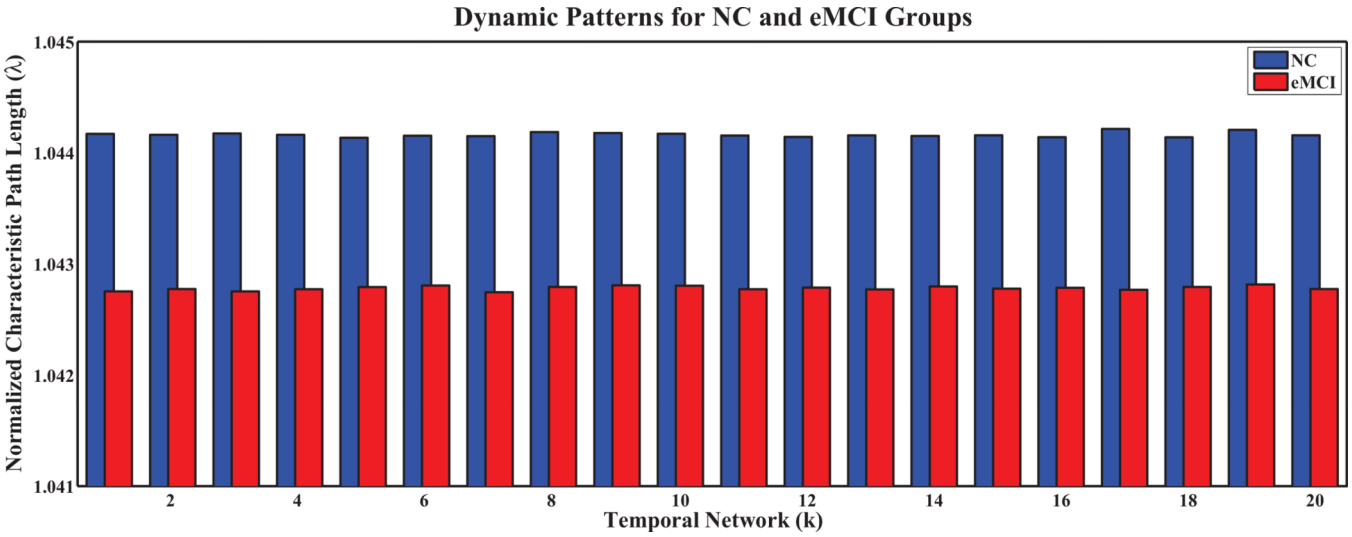

Fig. 8.

Normalized characteristic path lengths of temporal networks for eMCI and NC groups with $s = 2$ and $N = 90$.

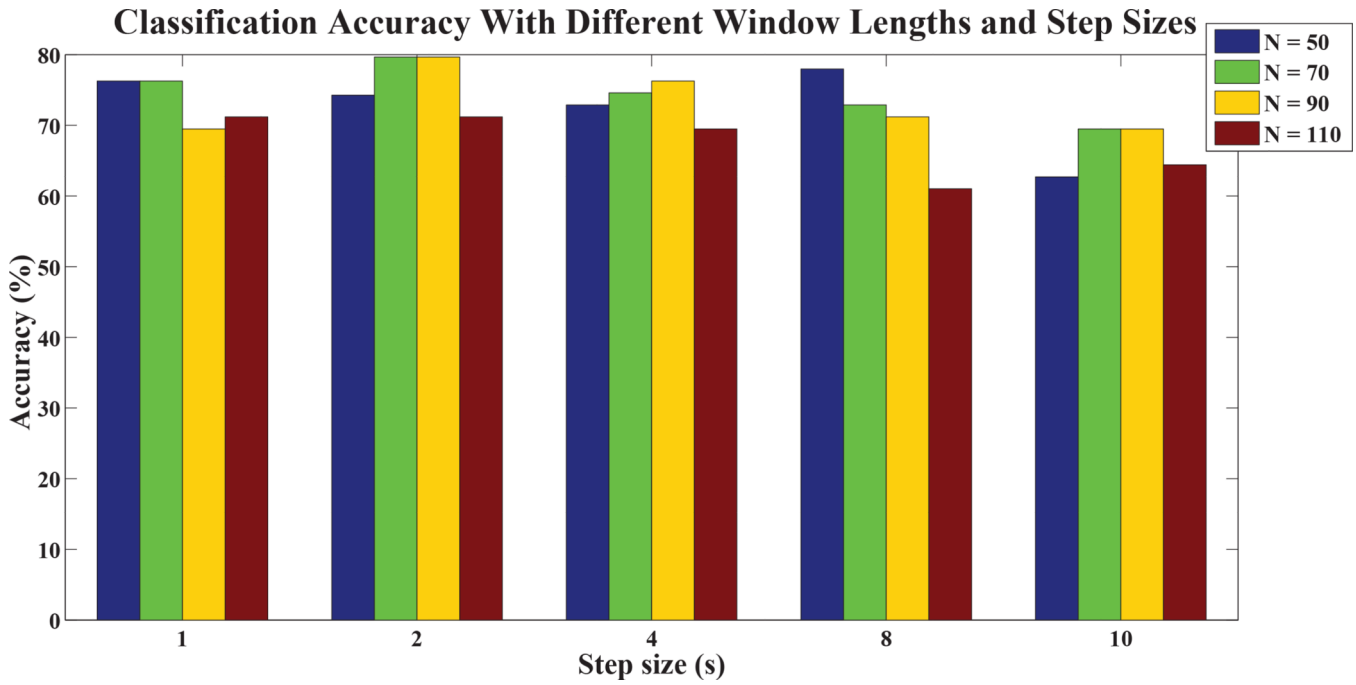

Fig. 9.
eMCI identification performance with respect to different window lengths and step sizes.

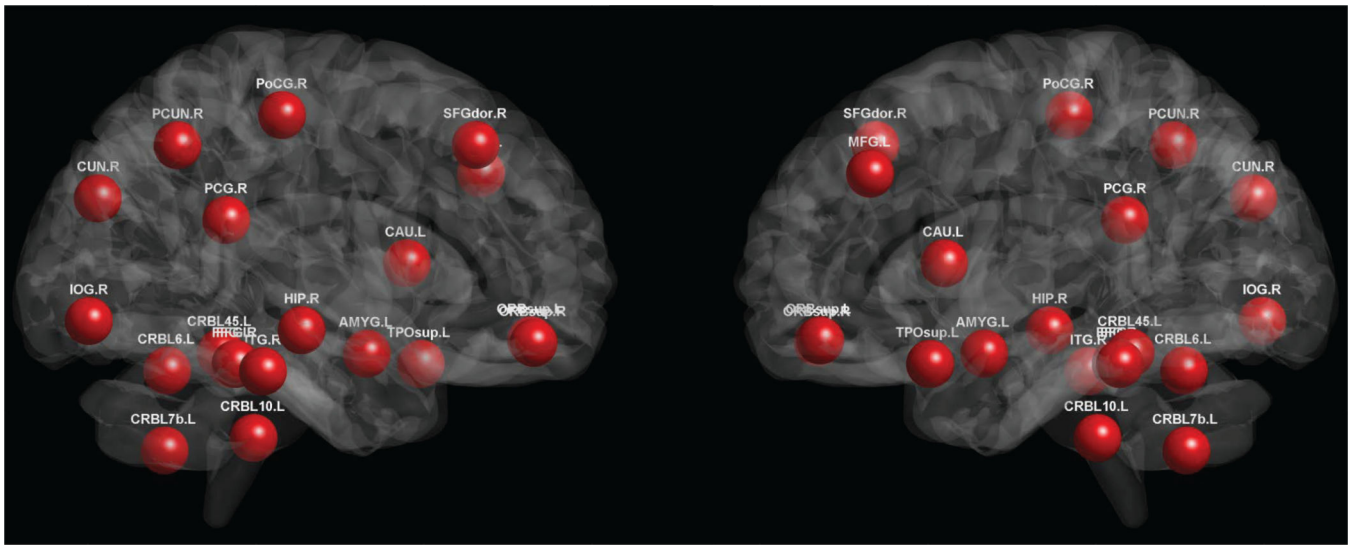

Fig. 10.

Most discriminative regions that were selected for eMCI classification. The colors indicate different ROIs.

Table 1

eMCI identification performance of the PAC-, PEC-, SICE-, GGL- and the proposed sparse temporal network-based frameworks with $N = 90$ and $s = 2$.

Method	ACC	AUC	SEN	SPE	Youden	F-score	BAC
PAC	0.6271	0.6598	0.6552	0.6000	0.2552	0.6333	0.6276
PEC	0.6610	0.6138	0.5517	0.7667	0.3184	0.6154	0.6592
SICE	0.6780	0.7189	0.6897	0.6667	0.3563	0.6780	0.6782
GGL	0.7288	0.7315	0.7586	0.7000	0.4586	0.7333	0.7293
Proposed	**0.7966**	**0.7920**	**0.7586**	**0.8333**	**0.5920**	**0.7857**	**0.7920**

(ACC = ACCuracy; AUC = Area Under ROC Curve; SEN = SENsitivity; SPE = SPEcificity; Youden = Youden Index; F-score = F score; BAC = Balance ACcuracy)